

Vortices in self-gravitating gaseous discs

G. R. Mamatsashvili^{1,2*} and W. K. M. Rice¹

¹*SUPA, Institute for Astronomy, University of Edinburgh, Blackford Hill, Edinburgh EH9 3HJ*

²*Georgian National Astrophysical Observatory, Il. Chavchavadze State University, 2a Kazbegi Ave., Tbilisi 0160, Georgia*

Accepted 2009 January 9. Received 2009 January 8; in original form 2008 November 6

ABSTRACT

Vortices have recently received much attention in the research of planet formation, as they are believed to play a role in the formation of km-sized planetesimals by collecting dust particles in their centres. However, vortex dynamics is commonly studied in non-self-gravitating discs. The main goal here is to examine the effects of disc self-gravity on vortex dynamics. For this purpose, we employ the 2D shearing sheet approximation and numerically solve the basic hydrodynamic equations together with Poisson's equation to take care of disc self-gravity. A simple cooling law with a constant cooling time is adopted, such that the disc settles down into a quasi-steady gravitoturbulent state. In this state, vortices appear as transient structures undergoing recurring phases of formation, growth to sizes comparable to a local Jeans scale and eventual shearing and destruction due to the combined effects of self-gravity (gravitational instability) and background Keplerian shear. Each phase typically lasts about two orbital periods or less. As a result, in self-gravitating discs, the overall dynamical picture of vortex evolution is irregular consisting of many transient vortices at different evolutionary stages and, therefore, with various sizes up to the local Jeans scale. By contrast, in the non-self-gravitating case, long-lived vortex structures persist for hundreds of orbits via merging of smaller vortices into larger ones until eventually their size reaches the disc scale height. Vortices generate density waves during evolution, which turn into shocks. This phenomenon of wave generation by vortices is an inevitable consequence of the differential character (shear) of disc rotation. Therefore, the dynamics of density waves and vortices are coupled implying that, in general, one should consider both vortex and spiral density wave modes in order to get a proper understanding of self-gravitating disc dynamics.

Our results suggest that given such an irregular and rapidly varying character of vortex evolution in self-gravitating discs, it may be difficult for such vortices to effectively trap dust particles in their centres, which is an alternative mechanism recently proposed for planetesimal formation. Further study of the behaviour of dust particles embedded in a self-gravitating gaseous disc is, however, required to strengthen this conclusion.

Key words: accretion, accretion discs – gravitation – hydrodynamics – instabilities – turbulence – planetary systems: protoplanetary discs.

1 INTRODUCTION

Research in protoplanetary disc dynamics is mainly focused on investigating the dynamical activities of two basic types/modes of perturbations – spiral density waves and vortices. They provide a means of outward angular momentum transport necessary for the secular evolution of a neutral disc, where the magnetorotational instability cannot operate. However, each mode is analysed for different settings: spiral density waves are the central perturbation types

and, therefore, the main agents responsible for angular momentum transport in self-gravitating discs, while vortices are commonly studied in non-self-gravitating discs. The formation and dynamics of vortices in protoplanetary discs has only recently attracted attention because of the role they may play in planet formation. The latest developments in non-self-gravitating discs have revealed that vortices can be (linearly) coupled with spiral density waves. This noteworthy finding, in turn, calls for revisiting self-gravitating disc dynamics with a particular emphasis on the possible role of vortical perturbations in the overall dynamical picture together with spiral density waves. Below we first outline the recent results on the vortex dynamics in astrophysical discs.

*E-mail: grm@roe.ac.uk

It has been demonstrated in both 2D global (Bracco et al. 1999; Godon & Livio 1999a,b; Davis, Sheehan & Cuzzi 2000; Godon & Livio 2000; Li et al. 2001; Davis 2002; Klahr & Bodenheimer 2003; Bodo et al. 2007) and local shearing sheet (Umurhan & Regev 2004; Barranco & Marcus 2005; Johnson & Gammie 2005; Shen, Stone & Gardiner 2006; Lithwick 2007) simulations of non-self-gravitating discs that only anticyclonic vortices (rotating in the same sense as the background shear) can survive in discs, though due to compressibility and/or viscosity they slowly decay on the time-scale of several hundred orbital periods. Nevertheless, anticyclonic vortices can be thought of as long-lived structures. On the other hand, cyclonic vortices get strongly sheared by differential rotation of the disc and eventually disappear. Simulations are often initiated with either random potential vorticity (PV) perturbations, which contain positive (cyclonic) and negative (anticyclonic) values in equal portions, or an imposed single vortex. The former shows that initial small-scale regions where PV is negative (anticyclonic regions) first get sheared into strips and then start to wrap up into small-scale vortices due to the specific instability discussed below. The latter gradually grow in size via merging into larger vortices until eventually their size becomes of the order of the disc scale height (Johnson & Gammie 2005); growth beyond this scale is restricted by compressibility effects. The initial small-scale cyclonic regions instead of wrapping up into distinct vortices get strongly sheared into strips and remain so during the entire course of evolution. This limitation on the vortex size was also confirmed in detailed simulations of a single vortex in a Keplerian disc (Bodo et al. 2007). In these simulations, a vortex with an initial length exceeding the disc scale height undergoes non-linear adjustment, during which it decreases in size radiating excess energy in the form of spiral density waves and shocks, and finally settles down to scales equal to a few disc scale height. These final scales are independent of the initial vortex size and determined by disc properties (sound speed and disc scale height).

The emission of spiral density waves by vortices during the adjustment process is due to the background Keplerian shear that ensures (linear) coupling between these two modes when the horizontal scale of vortices is equal to or larger than the disc scale height (Li et al. 2001; Davis 2002; Bodo et al. 2005; Johnson & Gammie 2005; Bodo et al. 2007; Mamatsashvili & Chagelishvili 2007). On the other hand, this condition is nothing more than the validity of 2D treatment. So, in the 2D case, compressibility is a key feature that must be taken account of. In this respect, all the results of 2D incompressible simulations of vortices should be regarded as approximate and less realistic. Emitted spiral density waves steepen into shocks afterwards and, hence, vortices appear to generate shocks that may play an important role in the outward transport of angular momentum, particularly in neutral discs where the magnetorotational instability cannot operate (see e.g. Li et al. 2001; Davis 2002; Johnson & Gammie 2005).

The basic underlying mechanism/instability responsible for the development of vortices as well as the necessary criterion for that were identified by Lithwick (2007) for incompressible shear flows. He interprets it as non-linear Kelvin–Helmholtz instability of a vortex strip with vorticity of the same sign as the background vorticity (for incompressible flows vorticity and PV are equivalent); for a vortex strip with the opposite sign of vorticity, no such instability is observed. This readily explains why cyclonic vortices cannot survive. This mechanism of vortex formation should be extended to compressible shear flows as well. Note that in this scenario one needs PV perturbations (e.g. vortex strips or random type) initially present in a disc. Other mechanisms of vortex, or PV, generation that

do not necessarily require this include inhomogeneities of entropy (temperature) distribution of a disc and are known as baroclinic instability (Klahr & Bodenheimer 2003; Klahr 2004; Petersen, Julien & Stewart 2007) and Rossby wave instability (Lovelace et al. 1999; Li et al. 2001).

Another important property of anticyclonic vortices – their dust trapping capability – was also investigated (e.g. Barge & Sommeria 1995; Chavanis 2000; Godon & Livio 2000; de la Fuente Marcos & Barge 2001; Johansen, Andersen & Brandenburg 2004; Inaba & Barge 2006; Klahr & Bodenheimer 2006). It has been shown that a smooth, sufficiently long-lived vortex is indeed able to effectively trap dust particles in its core, possibly accelerating planetesimal formation.

All the above-mentioned studies on vortex dynamics miss out an important aspect of protoplanetary discs – self-gravity (see reviews by Adams & Lin 1993; Durisen et al. 2007; Lodato 2007 on the role of self-gravity in protoplanetary disc dynamics). Typically, in discs, effective cooling times are too long to cause fragmentation under the action of their own self-gravity (Boley et al. 2006). As a consequence, balance is established between heating due to gravitational instability and cooling (self-regulation mechanism, Bertin & Lodato 2001). Discs are expected to stay in this self-regulated quasi-steady gravitoturbulent state for a long time. In this case, Toomre parameter hovers on the margin of gravitational instability. The properties of this state were numerically investigated in a large number of papers (e.g. Laughlin & Bodenheimer 1994; Laughlin, Korchagin & Adams 1997; Nelson, Benz & Ruzmaikina 2000; Gammie 2001; Johnson & Gammie 2003; Rice et al. 2003; Lodato & Rice 2004, 2005; Mejia et al. 2005; Boley et al. 2006; Stamatellos & Whitworth 2008, and references therein). A general dynamical picture is that spiral structure develops in a disc and transports angular momentum outwards through gravitational and hydrodynamic stresses, thereby allowing matter to accrete on to the central star. The angular momentum transport in this case is attributed to spiral density waves, which are thought of as the only perturbation type present in the disc. In other words, almost all studies on self-gravitating disc dynamics concentrate on the dynamical activity of spiral density waves and leave another class of perturbations – vortices – out of consideration. As discussed above, the latter plays an important role in non-self-gravitating discs and it seems natural to look for them and analyse their non-linear development in self-gravitating discs too. Indeed, in the linear theory it has already been shown that the coupling between spiral density wave and vortex modes is even more efficient in the presence of self-gravity (Mamatsashvili & Chagelishvili 2007). In perspective, this study will allow us to see if the same mechanism of planetesimal formation – dust particle trapping by vortices – can also be at work in self-gravitating discs.

In order to study the dynamics of vortical perturbations in self-gravitating discs, one must examine the behaviour of the PV field – the basic quantity characterizing vortex development. To date, no systematic investigation of PV behaviour, similar to that done for non-self-gravitating discs, has been carried out for self-gravitating ones. However, we should mention two relevant works by Adams & Watkins (1995) and Wada, Meurer & Norman (2002).

Adams & Watkins (1995) investigated the dynamics of a single vortex in the quasi-geostrophic and local shearing sheet approximations in a self-gravitating Keplerian disc. The quasi-geostrophic approximation implies that the characteristic time-scale of a problem is much larger than the orbital period. The vortex considered in their paper is in geostrophic balance and, therefore, remains steady for many rotation periods. The gas motion inside the vortex is subsonic as well. In this case, the effect of self-gravity is only to

make the effective length-scale (Rossby radius) of the vortex larger than that in the non-self-gravitating case. The quasi-geostrophic approximation does not permit consideration of the most important aspect of dynamics – compressibility effects (spiral density waves and shocks), which are intertwined with vortices and have typical time-scales of the order of orbital (shear) time. In other words, these relatively fast motions associated with compressibility are filtered out in this approximation.

Wada et al. (2002) investigated the properties of the gravitoturbulent state in the interstellar medium of galaxies. The vorticity (but not PV) field in this state is indeed calculated in their paper, which has a rather complicated structure. However, the authors do not discuss in detail the properties of the vorticity field and its relation to the density and pressure fields. They only point out that negative and positive vorticity regions are associated with dense filaments seen in the density field. In that paper, the main emphasis is placed on analysing the spectral properties of gravitoturbulence. Their study clearly demonstrates that vortical perturbations are as important as spiral density waves in the formation of spectra of the resulting gravitoturbulent state.

In this paper, following the approach adopted by Gammie (2001) and Johnson & Gammie (2005), we study the specific properties of vortex, or PV, evolution in self-gravitating discs by means of numerical simulations. We work in the 2D shearing sheet approximation (Goldreich & Lynden-Bell 1965; Goldreich & Tremaine 1978) without invoking the quasi-geostrophic approximation, thereby allowing for compressibility effects. In this respect, our analysis is more general than that of Adams & Watkins (1995). In addition, we do not impose a single vortex in geostrophic balance in the beginning. Instead, we start with random perturbations of velocity components, and hence of PV, and trace the development of structures out of this chaotic field. These chaotic initial perturbations are more realistic than a single vortex. *The main focus here is on the dynamical picture of PV evolution in the state of quasi-steady gravitoturbulence and how this picture differs from that occurring in non-self-gravitating discs given the same chaotic type of initial conditions.* This, in turn, allows us to draw important conclusions about the effects of self-gravity on the formation and evolution of vortices. We will see that in the presence of self-gravity, vortex evolution is not as smooth and regular as it is in the non-self-gravitating case. This study is actually an extension to the non-linear regime with added cooling of Mamatsashvili & Chagelishvili (2007), where we carried out linear analysis of the transient growth and coupling of vortices and spiral density waves in self-gravitating discs.

The paper is organized as follows. Physical approximations and the mathematical formalism of the problem as well as the numerical techniques used are introduced in Section 2, non-linear evolution of the fiducial model and the comparative study of correlation functions for different models are described in Section 3 and summary and discussions are given in Section 4.

2 PHYSICAL MODEL AND EQUATIONS

In order to study the evolution of vortices in thin self-gravitating gaseous discs, we employ the 2D local shearing sheet model. This model represents a simple analogue to a differentially rotating disc and has an advantage over global disc models in that it permits higher resolution study of dynamical processes in discs. In the shearing sheet model, disc dynamics is studied in the local Cartesian coordinate frame corotating with the angular velocity of disc rotation at some radius from the central star. In this coordinate frame, the unperturbed differential rotation of the disc manifests

itself as a parallel azimuthal flow \mathbf{u}_0 with a constant velocity shear in the radial direction. The unperturbed background surface density Σ_0 and 2D pressure P_0 corresponding to this shear flow are assumed to be spatially constant. A Coriolis force is also included to take into account the effects of the coordinate frame rotation. As a result, in this local approximation, the continuity equation and equations of motion take the form (Goldreich & Tremaine 1978; Gammie 2001)

$$\frac{\partial \Sigma}{\partial t} + \nabla \cdot (\Sigma \mathbf{u}) - q \Omega x \frac{\partial \Sigma}{\partial y} = 0, \quad (1)$$

$$\frac{\partial u_x}{\partial t} + (\mathbf{u} \cdot \nabla) u_x - q \Omega x \frac{\partial u_x}{\partial y} = -\frac{1}{\Sigma} \frac{\partial P}{\partial x} + 2\Omega u_y - \frac{\partial \psi}{\partial x}, \quad (2)$$

$$\frac{\partial u_y}{\partial t} + (\mathbf{u} \cdot \nabla) u_y - q \Omega x \frac{\partial u_y}{\partial y} = -\frac{1}{\Sigma} \frac{\partial P}{\partial y} + (q - 2)\Omega u_x - \frac{\partial \psi}{\partial y}. \quad (3)$$

This set of equations is supplemented with Poisson's equation for a razor-thin disc:

$$\Delta \psi = 4\pi G (\Sigma - \Sigma_0) \delta(z). \quad (4)$$

Here, $\mathbf{u}(u_x, u_y)$, P , Σ and ψ are, respectively, the perturbed velocity relative to the background parallel shear flow $\mathbf{u}_0(0, -q\Omega x)$, the 2D pressure, the surface density and the gravitational potential of the gas sheet. Since equations (2 and 3) are written for perturbed velocities, only the gravitational potential due to the perturbed surface density $\Sigma - \Sigma_0$ is used. In the dynamical equations, the gradients of the gravitational potential are taken at $z = 0$, i.e. where the shearing sheet is located, because only this quantity depends on the vertical coordinate z . Ω is the angular velocity of the coordinate frame rotation as a whole. x and y are, respectively, the radial and azimuthal coordinates. The shear parameter $q = 1.5$ for the Keplerian rotation considered in this paper.

The equation of state is

$$P = (\gamma - 1)U,$$

where U and γ are the 2D internal energy density and adiabatic index, respectively. We will adopt $\gamma = 2$ throughout.

The central quantity of this study is the vertical component of potential vorticity referred to as PV for short:

$$I \equiv \frac{\hat{z} \cdot \nabla \times \mathbf{u} + (2 - q)\Omega}{\Sigma} = \frac{1}{\Sigma} \left[\frac{\partial u_y}{\partial x} - \frac{\partial u_x}{\partial y} + (2 - q)\Omega \right],$$

where \hat{z} is the unit vector in the vertical direction. In the unperturbed state, where there is only the background Keplerian shear flow, \mathbf{u}_0 , with the constant equilibrium surface density Σ_0 , PV is equal to $I_0 = (2 - q)\Omega/\Sigma_0$. The PV will play an important role in the subsequent analysis, as it generally characterizes the formation of coherent structures (vortices) in a disc flow (e.g. Godon & Livio 1999a,b; Johnson & Gammie 2005; Bodo et al. 2007). Using equations (1–3), after some algebra, one can show that the evolution of PV is governed by the following equation:

$$\left(\frac{\partial}{\partial t} + \mathbf{u} \cdot \nabla - q \Omega x \frac{\partial}{\partial y} \right) I = \frac{1}{\Sigma^3} \left(\frac{\partial \Sigma}{\partial x} \frac{\partial P}{\partial y} - \frac{\partial \Sigma}{\partial y} \frac{\partial P}{\partial x} \right).$$

This equation describes the advection of PV along the trajectories of fluid elements (Lagrangian derivative inside the brackets on the left-hand side) and its change due to the non-linear baroclinic term on the right-hand side. In the present case, the pressure and surface density are not related by any (e.g. isentropic, isothermal or polytropic) constraint, so this baroclinic term is, in general, non-zero and, therefore, PV is not conserved. However, in the linear approximation it vanishes and PV is conserved making it possible

to classify modes into vortical and wave types (Mamatsashvili & Chagelishvili 2007). Also note that the gravitational potential, as it should be, does not explicitly enter into this equation; self-gravity only influences PV evolution through surface density, pressure and velocity fields.

The evolution of internal energy density is governed by the equation:

$$\frac{\partial U}{\partial t} + \nabla \cdot (U\mathbf{u}) - q\Omega x \frac{\partial U}{\partial y} = -P\nabla \cdot \mathbf{u} - \frac{U}{\tau_c}, \quad (5)$$

where the first term on the right-hand side is the compressional heating term and the second term takes into account cooling of the disc. Here, we assume the cooling time τ_c to be constant and choose its value so that the disc does not fragment and achieves a saturated state, where all quantities fluctuate around constant average values. Namely, we take $\tau_c = 20\Omega^{-1}$, which means a non-fragmenting disc according to Gammie's (2001) criterion.¹ We refer to this quasi-steady state as gravitoturbulence. *In this study, we concentrate on examining the specific properties of PV evolution in such a gravitoturbulent state.* Where fragmentation conditions are concerned, more realistic cooling laws, with τ_c being a function of Σ , U , Ω rather than a constant, are necessary (e.g. Johnson & Gammie 2003; Boley et al. 2006). Most simulations of self-gravitating discs with such a realistic cooling, however, indicate that in this case cooling is usually not sufficient to cause fragmentation over most of the disc except possibly for the outer regions, therefore, a quasi-steady state is more likely (see review by Durisen et al. 2007). We do not include any artificial heating terms in the internal energy equation; heating is solely due to the compressional term and shocks captured by means of artificial (von Neumann-Richtmyer) viscosity in our code.

2.1 Numerical methods

Our computational domain in the (x, y) plane is a rectangle $-L_x/2 \leq x \leq L_x/2$, $-L_y/2 \leq y \leq L_y/2$ of size $L_x \times L_y$ divided into $N_x \times N_y$ grid cells. The numerical resolution is therefore $\Delta x \times \Delta y = L_x/N_x \times L_y/N_y$. We will assume that $L_x = L_y \equiv L$ and $N_x = N_y \equiv N$. For the fiducial model presented below we take $N = 1024$, though we also ran a lower resolution ($N = 512$) model that converges to the fiducial model. In order to integrate the governing equations (1–5) within this domain, we use a version of the ZEUS code (Stone & Norman 1992), which is more suited to the shearing sheet (Gammie 2001; Johnson & Gammie 2003, 2005). ZEUS evolves these equations on a staggered mesh in a time-explicit, operator-split, finite-difference fashion. As mentioned above, the code uses artificial viscosity to capture shocks.

The transport scheme differs from that of the basic ZEUS algorithm. To show this, in the left-hand side of equations (1–5) we have explicitly decomposed the advection of physical quantities by the flow into two parts: the first one (with $\mathbf{u} \cdot \nabla$) represents advection by the perturbed velocity and is done using the van Leer algorithm for calculating fluxes of conserved quantities as in the original ZEUS algorithm. The second one (with $-q\Omega x \partial/\partial y$) describes the advection by the background Keplerian shear flow \mathbf{u}_0 and is done by means of the FARGO scheme (Masset 2000) with the use of the same van Leer algorithm for performing the fractional part of the shift; the integral part of the shift is done by a simple remap. This scheme has the advantage that it allows larger than standard

integration time-steps by removing the background shear flow from the Courant condition, which severely limits the time-step because of large shear velocities at the x -boundaries. Now only the perturbed velocity \mathbf{u} , rather than the full velocity $\mathbf{u}_0 + \mathbf{u}$, enters this condition. Numerical diffusion of the code is also reduced by this procedure.

As with most works employing shearing sheet approximation, we adopt periodic boundary conditions in the y -direction and shearing periodic in the x -direction, that is, the x -boundaries are initially periodic but as time goes by they shear with respect to each other becoming again periodic when $t_n = nL_y/(q\Omega L_x) = n/(q\Omega)$, with $n = 1, 2, \dots$. So, for each variable, we can write

$$f(x, y, t) = f(x, y + L, t) \quad (y \text{ boundary})$$

$$f(x, y, t) = f(x + L, y - q\Omega L t, t) \quad (x \text{ boundary}),$$

where $f \equiv (u_x, u_y, P, \Sigma, U)$. The way of implementing these shearing sheet boundary conditions is described in detail in Hawley, Gammie & Balbus (1995). The shearing in the x -boundary conditions, or shift in the y -direction by an amount $-q\Omega L t$ in the 'ghost zones', is done here by means of the FARGO algorithm.

We define the autocorrelation function for PV as

$$R_I(x, y) = \frac{\Sigma_0^2}{\Omega^2 L_x L_y} \int \delta I(x', y') \delta I(x + x', y + y') dx' dy',$$

where the integration is over the entire rectangular simulation domain and $\delta I = I - I_0$. The autocorrelation function characterizes emerged coherent structures in a flow; its length-scale can be identified with the characteristic scale of such structures. An analogous function was used by Gammie (2001) to analyse density structures in order to establish locality of angular momentum transport and by Johnson & Gammie (2005) to characterize coherent vortices in the non-self-gravitating shearing sheet.

Our method of solving Poisson's equation is analogous to that used by Johansen et al. (2007) and differs from the original method of Gammie (2001) in the following respect. In Gammie (2001), the surface density is first linearly interpolated on to a grid of shearing coordinates $[x' = x, y' = y + q\Omega x(t - t_p)]$, $t_p = (q\Omega)^{-1} NINT(q\Omega t)$, where it is exactly periodic, and then Fourier transformed with a standard Fast Fourier Transform (FFT) technique. After that the Fourier transform of the gravitational potential is found from the Poisson's equation rewritten in wavenumber (k_x, k_y) plane:

$$\psi(k_x, k_y, t)|_{z=0} = -\frac{2\pi G \Sigma(k_x, k_y, t)}{\sqrt{[k_x + q\Omega k_y(t - t_p)]^2 + k_y^2}},$$

where $\psi(k_x, k_y, t)|_{z=0}$ and $\Sigma(k_x, k_y, t)$ are the Fourier transforms of the gravitational potential and surface density with the background constant value subtracted. The potential is then transformed back into the grid of shearing coordinates and finally linearly interpolated on to the grid of (x, y) coordinates. We instead Fourier transform directly from the (x, y) plane to the (k_x, k_y) plane and vice versa without doing an intermediate transformation to the shearing coordinates. However, in this case we take into account the fact that the radial wavenumber k_x of each spatial Fourier harmonic is no longer constant, but changes with time as $k_x(t) = k_x(0) + q\Omega k_y t$ in order to remain consistent with the shearing sheet boundary conditions discussed above. As a consequence, at each time t in the corresponding computational domain in the (k_x, k_y) plane there are only Fourier harmonics with wavenumbers $k_y = 2\pi n_y/L$, $k_x = 2\pi n_x/L + q\Omega t' (2\pi n_y/L)$, where $t' = \text{mod}[t, 1/(q\Omega|n_y|)] [\text{mod}(a, b)$ is modulus after dividing a by b] and integer numbers n_x, n_y lie in the interval $-N/2 \leq n_x, n_y \leq N/2$. So, when doing Fourier (inverse Fourier) transform, we decompose (sum) into (over) these

¹We also checked that as long as a disc does not fragment, different values of the cooling time do not qualitatively change results.

wavenumbers. We accordingly modified the standard FFT routine to perform this decomposition (summation). In some sense, it is equivalent to changing from the (x', y') plane to the (x, y') plane via Fourier transformation, which is more exact than that done by linear interpolation.² In order to make the gravitational force isotropic on small scales, we keep only harmonics with $k < \pi N/(L\sqrt{2})$, where $k = (k_x^2 + k_y^2)^{1/2}$. We have checked using the linear shearing wave test that the present version of potential solver gives more accurate results than that used previously.

This version of the ZEUS code was tested on linear problems involving shearing (vortical and compressible) waves in the (non)-self-gravitating shearing sheet (Gammie 2001; Johnson & Gammie 2005). The code results are in an excellent agreement with those of the linear theory until the decreasing radial wavelength of shearing waves becomes comparable to the grid cell size. So, we do not give these basic tests here and refer the interested reader to the above papers.

2.2 Total energy equation and α parameter

In this subsection, we derive a relationship between the total energy and hydrodynamic and gravitational stresses. This relationship is important as it clearly shows the role of shear in the energy exchange between the background Keplerian flow and perturbations. The total energy density of perturbed (from Keplerian shear flow) gas motion is defined as

$$E = \frac{1}{2} \Sigma \mathbf{u}^2 + U + \frac{1}{2} (\Sigma - \Sigma_0) \psi,$$

where the first term is the kinetic energy density, the second term, as defined above, is the internal energy density and the third term is the gravitational energy density. Using basic equations (1–5) and the shearing sheet boundary conditions, the equation for the average total energy is

$$\frac{d\langle E \rangle}{dt} = q\Omega \left\langle \Sigma u_x u_y + \frac{1}{4\pi G} \int_{-\infty}^{+\infty} \frac{\partial \psi}{\partial x} \frac{\partial \psi}{\partial y} dz \right\rangle - \frac{\langle U \rangle}{\tau_c},$$

where the angle brackets denote averages defined as $\langle f \rangle = \int f dx dy / L_x L_y$, where the integration is done over the entire simulation domain. The first and second terms inside the angle brackets on the right-hand side are Reynolds and gravitational stresses, respectively. As is clear from this equation, these two terms are responsible for the energy exchange between the background Keplerian flow and perturbations, which is in fact possible due to the differential nature (shear) of Keplerian rotation. In the absence of background shear ($q = 0$), the total energy of perturbations changes only due to cooling. Incidentally, the sum in the angle brackets is also proportional to the angular momentum flux density (Gammie 2001). Since the cooling time is not short enough, the system, as mentioned above, settles into a quasi-steady gravitoturbulent state in which $d\langle E \rangle/dt = 0$ (similarly for every average variable). Therefore, at these times we can write

$$q\Omega \left\langle \Sigma u_x u_y + \frac{1}{4\pi G} \int_{-\infty}^{+\infty} \frac{\partial \psi}{\partial x} \frac{\partial \psi}{\partial y} dz \right\rangle = \frac{\langle U \rangle}{\tau_c},$$

or in terms of the well-known α viscosity parameter

$$\alpha \equiv \frac{1}{\langle \Sigma c_s^2 \rangle} \left\langle \Sigma u_x u_y + \frac{1}{4\pi G} \int_{-\infty}^{+\infty} \frac{\partial \psi}{\partial x} \frac{\partial \psi}{\partial y} dz \right\rangle$$

giving

$$\alpha = \frac{1}{q\gamma(\gamma - 1)\Omega\tau_c}, \quad (6)$$

where c_s is the adiabatic sound speed defined as $c_s^2 = \gamma P / \Sigma = \gamma(\gamma - 1)U / \Sigma$. This relation is very important, as it shows that if a quasi-steady state can be achieved, then angular momentum transport must be determined solely by the cooling time for a given rotation rate and, therefore, should be constant with time. (The same formula for α was derived by Gammie 2001 in a different way.) It is the local analogue of the result that the surface brightness of the disc does not depend on the details of the angular momentum transport mechanism. Again, the basic premise here is the possibility of the existence of a quasi-steady gravitoturbulent state, which is able to feed itself, or be self-sustained, at the expense of background shear flow energy extracted by Reynolds and gravitational stresses. In the presence of disc self-gravity and cooling, this state is easily reached because of the self-regulation mechanism (Bertin & Lodato 2001). However, in thin 2D models of non-self-gravitating neutral discs steady outward angular momentum transport is hard to achieve. In this case typically the disc is unstable to vortex formation and develops well-organized vortices, which, although able to transport angular momentum outwards mostly via generating compressible motions (shocks), are still slowly decaying on the time-scale of several hundred orbital periods (e.g. Johnson & Gammie 2005; Shen et al. 2006). Thus, the role of self-gravity and cooling is crucial for the maintenance of gravitoturbulence.

Before proceeding to the main analysis, we introduce non-dimensional variables. As mentioned above, in the unperturbed state the background surface density Σ_0 , pressure P_0 and internal energy U_0 are all spatially constant. In the unperturbed state, the sound speed is $c_{s0}^2 = \gamma P_0 / \Sigma_0 = \gamma(\gamma - 1)U_0 / \Sigma_0$. We switch to non-dimensional variables: $t \rightarrow \Omega t$, $(x, y) \rightarrow (x\Omega/c_{s0}, y\Omega/c_{s0})$, $(k_x, k_y) \rightarrow (k_x c_{s0}/\Omega, k_y c_{s0}/\Omega)$, correspondingly the computational domain size $L \rightarrow L\Omega/c_{s0}$, $(u_x, u_y, c_s) \rightarrow (u_x/c_{s0}, u_y/c_{s0}, c_s/c_{s0})$, $\Sigma \rightarrow \Sigma/\Sigma_0$, $(P, U, E) \rightarrow (P/c_{s0}^2 \Sigma_0, U/c_{s0}^2 \Sigma_0, E/c_{s0}^2 \Sigma_0)$, $\psi \rightarrow \psi/c_{s0}^2$, $I \rightarrow I\Sigma_0/\Omega$. Note that c_{s0}/Ω is actually the scale height of the disc. Therefore, distances are normalized by the disc scale height. The local Mach number is defined as $M = \sqrt{u_x^2 + u_y^2}/c_s$. The Toomre parameter, a measure of the self-gravity of a disc, is $Q = c_s \Omega / \pi G \Sigma$ (Toomre 1964). These non-dimensional variables are used from now on throughout the paper. In the simulations presented below, we start with $Q = Q_0 = c_{s0} \Omega / \pi G \Sigma_0 = 1.5$.

2.3 Initial conditions

The initial conditions consist of random u_x and u_y perturbations superimposed on the mean Keplerian shear flow. The surface density and internal energy are not perturbed initially and thus are spatially uniform with values 1 and $1/\gamma(\gamma - 1)$, respectively. To generate these initial conditions, for each velocity component at each point in the (k_x, k_y) plane, we create a Gaussian random field with standard deviation, or amplitude of power spectrum, given by the Kolmogorov power law $|u_{x,y}(k_x, k_y)|^2 \sim k^{-8/3}$, $k = \sqrt{k_x^2 + k_y^2}$, in the range $k_{\min} \leq k \leq k_{\max}$. The limits of this range are $k_{\min} = 2\pi/L$ and $k_{\max} = (N/n_g)k_{\min}$, where n_g is the number of grid cells contained within the smallest wavelength $2\pi/k_{\max}$ for which we choose $n_g = 16$ when $N = 1024$. Outside this wavenumber range, the power spectrum is set to zero. This random field is then transformed back into the real (x, y) plane. For the amplitude of velocity perturbations $\sigma = \langle \mathbf{u}^2 \rangle^{1/2}$, we initially take $\sigma = 0.6$. Fig. 1 shows

²See website <http://imp.mcmaster.ca/~colinn/ism/rotfft.html>.

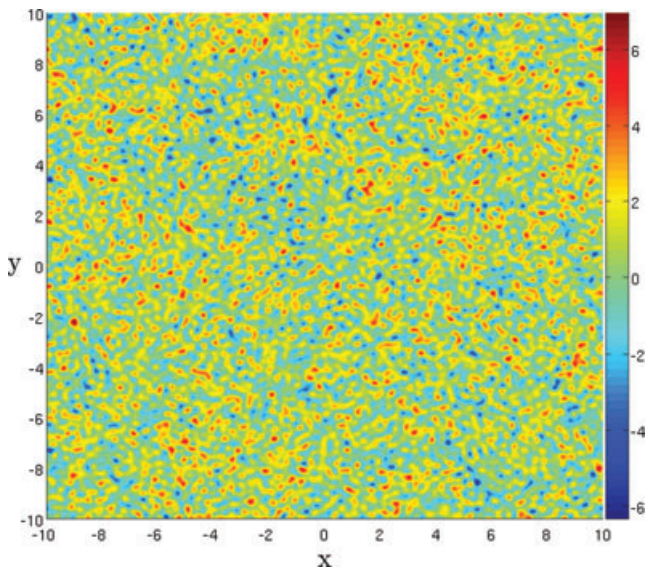


Figure 1. Initial (at $t = 0$) distribution of PV in the real plane corresponding to a Kolmogorov spectrum in wavenumber plane for the fiducial model with $L = 20$. Both negative (blue and light blue) and positive (yellow and red) values of PV are present (see electronic version of the journal for colour figures).

these initial conditions in terms of PV in the real plane. From this figure, we can see that in the real plane the initial PV field has a chaotic character with equal contributions from negative and positive values. Although we start with a Kolmogorov power spectrum, a general dynamical picture emerging in the quasi-steady state does not depend strongly on the initial conditions. These random velocity perturbations are meant to mimic the turbulent state in a disc resulting from the collapse of a molecular cloud (Godon & Livio 2000).

Note that we do not impose any constraints on the initial fields u_x and u_y , such as the requirement of incompressibility ($\nabla \cdot \mathbf{u} = 0$) adopted by Johnson & Gammie (2005) and Shen et al. (2006) to pick out only vortical perturbations; so these two velocity components are not correlated. We found that the mere presence of negative PV values in initial conditions is sufficient for the development of vortices, even though they may also contain some fraction of wave perturbations. Linear analysis (Mamatsashvili & Chagelishvili 2007) shows that, in shear flows, vortical perturbations become divergent if they are initially non-divergent and wave perturbations become rotational (with non-zero velocity curl) due to the background velocity shear. But wave perturbations never acquire PV if it is not present initially (of course, here we assume that there are no baroclinic terms in the PV equation in the linear approximation, or equivalently unperturbed surface density and pressure are uniform). Thus, truly vortical perturbations should be characterized by non-zero PV even though they may develop divergence in the course of evolution. It is the PV that determines the vortex formation and it must be present initially. By choosing initial perturbed velocity field with a non-zero PV, we ensure the presence of vortical perturbations with a possible mix of wave perturbations with zero PV, which do not affect the vortex formation process. In other words, the class of initial conditions capable of causing vortex formation is broader; they must be characterized only by a non-zero negative PV and may not necessarily satisfy the incompressibility requirement, that is, they can comprise a fraction of wave perturbations as well. This alleviates the problem of vorticity injection. Initial conditions

resulting from the collapse of a molecular cloud into a disc, where PV is everywhere zero, would be somewhat contrived and therefore less likely.

3 NON-LINEAR EVOLUTION

In this section, we present the non-linear evolution of the fiducial model with size $L = 20$ starting with the initial conditions described in the previous section. We describe in detail the development of structures in the PV, surface density and pressure/internal energy fields. The size $L = 20$ corresponds to a minimum wavenumber $k_{y\min} = 0.314$ in the computation domain, for which linear swing growth is largest as a function of k_y , at $Q = 1.5$. Thus, we ensure that from the outset our computational domain comprises those scales for which self-gravity is important. In the presence of both strong Keplerian shear and self-gravity, the main mechanism responsible for the growth of initial velocity perturbations is swing amplification instead of pure Jeans instability. Swing amplification has a transient exponential nature because of the ‘drift’ of radial wavenumbers of spatial Fourier harmonics of perturbations through unstable regions in the (k_x, k_y) plane that are brought about by the combined action of shear and self-gravity (Toomre 1981; Kim & Ostriker 2001; Mamatsashvili & Chagelishvili 2007). As a result, the average values of various quantities undergo rapid amplification over a relatively short time interval (Figs 2 and 3; see also Gammie 2001). The evolution of the same quantities for a lower resolution $N = 512$ run is almost similar. The small difference between these two runs may be attributed to the specificity of PV, surface density and internal energy fields for different resolutions, see also Shen et al. (2006). We call this interval the burst phase. During swing amplification, the initial velocity perturbations induce strong surface density perturbations in the form of shocks with density contrast by a factor of about 100. These shocks have trailing orientation, because swing amplification always tends to produce trailing structures. The gas motion is also supersonic at this stage. It can be seen from Fig. 3 that the average and maximum Mach numbers reach largest values 1.1 and 7–8, respectively. Shock regions are the sources of intense

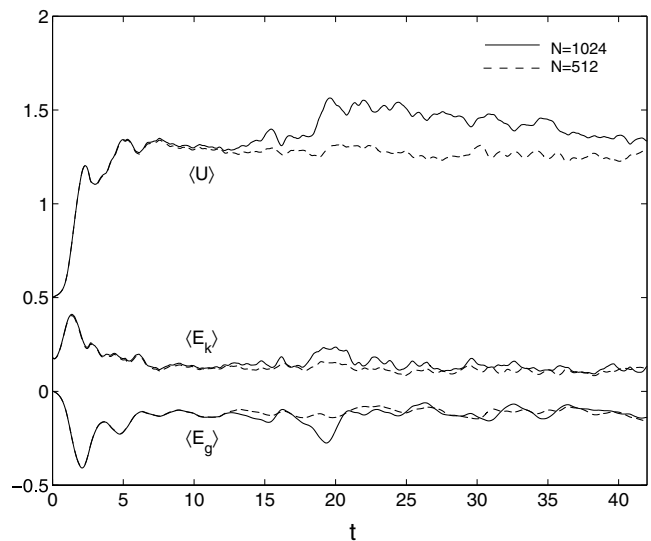


Figure 2. Evolution of the average kinetic, internal and gravitational energies. During the burst phase, they undergo rapid (swing) amplification until $t \approx 2$ –2.5 and then remain, on average, constant in the quasi-steady gravitoturbulent phase, which sets in at about $t = 5$. The evolution of the same quantities for a lower resolution ($N = 512$) run is similar.

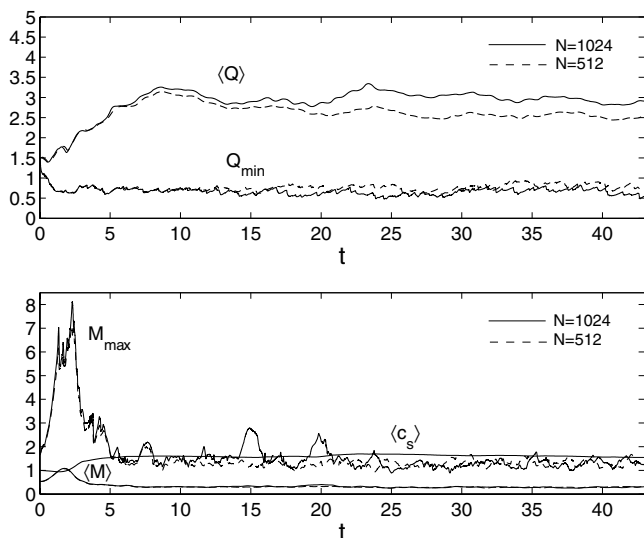


Figure 3. Evolution of $\langle Q \rangle$ and minimum Q_{\min} (upper plot) and the average Mach number $\langle M \rangle$, maximum M_{\max} and $\langle c_s \rangle$ (lower plot). $\langle Q \rangle$ initially rises due to strong shock heating in the burst phase, but then levels off at about three in the gravitoturbulent phase. Q_{\min} remains constant and low 0.6–0.7 implying that there are always unstable regions associated with negative PV, or vortices. $\langle M \rangle$ initially rises but then settles down to smaller values 0.3, so that gas motion is on average subsonic. However, M_{\max} remains of the order of unity showing that there is still some sonic motion. The average sound speed $\langle c_s \rangle$ also reaches a constant value in the gravitoturbulent phase.

heating of the gas together with compressional heating (the first term on the right-hand side of equation 5) and therefore the internal energy undergoes jumps in the shocks. Eventually, strong shocks heat the disc up, but cooling compensates for heating, so that at about $t = 5$ a quasi-steady gravitoturbulent state is reached, where the average kinetic, internal and gravitational energies as well as $\langle Q \rangle$, Q_{\min} , the average Mach number $\langle M \rangle$, the maximum Mach number M_{\max} and $\langle c_s \rangle$ fluctuate around constant values (Figs 2 and 3). At these times, the angular momentum transport parameter α is given by equation (6) and constant. Now $\langle M \rangle$ fluctuates around 0.3, so that, on average, the gas motion is subsonic, however, M_{\max} fluctuates around 1.24 meaning that the motion is still sonic mostly in the vicinity of shocks. $\langle Q \rangle$ fluctuates around 3, but we will see below that the $Q(x, y, t)$ field is very inhomogeneous containing values as small as 0.6–0.7 associated with negative PV regions (vortices).

In Fig. 4, we trace the parallel evolution of PV, surface density, pressure (the same as internal energy for $\gamma = 2$) and Q fields to identify correlations between them and to compare them with those in non-self-gravitating discs. We emphasize from the beginning that the evolution is not as smooth and regular as it is in the non-self-gravitating case. As we will see below, in self-gravitating discs, vortices are transient structures undergoing recurring phases of formation, growth and destruction, whereas in non-self-gravitating discs small-scale vortices once formed, gradually merge into larger vortices.

During the burst phase, initially small-scale positive and negative PV regions get strongly sheared into strips, but negative PV (anticyclonic) regions start to wrap up into vortex-like structures towards the end of the burst phase due to non-linear Kelvin–Helmholtz instability (Lithwick 2007). The positive PV regions remain sheared into strips showing no signs of vortex formation during the entire course of evolution. Thus, only anticyclonic regions are able to sur-

vive in shear flows by taking the form of vortices. As mentioned in the Introduction, this is a quite general result confirmed in many simulations of astrophysical as well as purely hydrodynamical contexts. As evident from Fig. 4, in the subsequent quasi-steady state, the overall dynamical picture of PV evolution is still irregular and varying on the dynamical time-scale. For this reason, throughout the paper, we use the term ‘vortex’ in a broader sense meaning generally a negative PV region and not only a vortex with a well-defined shape commonly occurring in non-self-gravitating discs. As demonstrated below, in a quasi-steady state, these negative PV regions are associated with underdense/underpressure and overdense/overpressure regions superimposed on the shocks that may be important for trapping dust particles.

Small-scale anticyclonic vortices initiated at the end of the burst phase continue to grow further in size in the quasi-steady saturated state which is reached, as mentioned, at about $t = 5$. Fig. 4 presents a typical dynamical picture of such a gravitoturbulent state, which is quasi-stationary and remains unchanged (on average) with time during the entire course of evolution. Vortices with a large (by absolute value) negative central value of PV (blue dots in the PV field) have more or less vortex-like shape and correspond to the central underdense regions surrounded by the higher density regions. Due to the background Keplerian shear, the total motion in the vicinity of such negative PV regions is a complex mixture of vortical and compressive (wave) motions giving rise to this type of density structure. In these enhanced density regions, PV is smaller by absolute value than that in the vortex centre. Thus, generally in shear flows the coupling with wave motions is typical of vortex dynamics irrespective of the disc being self-gravitating or not. These compressive motions turn into shocks afterwards that are also seen in the surface density and pressure fields (more precisely, the shock structure in these fields is a net result of non-linear superposition/mixture of shock waves emitted by such individual vortices). So, classifying perturbations into purely vortical – having only zero divergence and non-zero curl – and compressive – having only non-zero divergence and zero curl – is not quite appropriate, because due to background shear, divergence and curl become linked and change with time during the evolution that, in turn, causes mixing of these two perturbation types (Mamatsashvili & Chagelishvili 2007). With regard to angular momentum transport, it would be more exact to attribute it to the overall gas motion with non-zero PV and divergence rather than to compressive (wave) or vortical perturbations only.

A similar dynamical picture is also observed in the evolution/adjustment of a single vortex in a compressible non-self-gravitating Keplerian disc (Bodo et al. 2007). The vortex initially produces saddle-like density structure, much like observed in our simulations, with an underdense region at the location of the vortex centre surrounded by an overdense region with accompanying shock waves.

With time the effect of self-gravity on each vortex comes into play because of the growing length-scale of vortices, and at the same time of the increasing surface density/overdensity associated with them. The vortex growth in size is a consequence of inverse – towards larger scales – cascade of energy characteristic of 2D flows as clearly demonstrated in simulations (e.g. Godon & Livio 1999a). The amplification of the vortex surface density is again due to the swing mechanism. For the same reason that in self-gravitating discs perturbations experience considerably larger swing growth than in non-self-gravitating discs, the traces of vortices in the surface density field – the overdense regions around underdense regions – become more and more notable on the background of density variations related to shocks. From Fig. 4, it is seen that overdensities

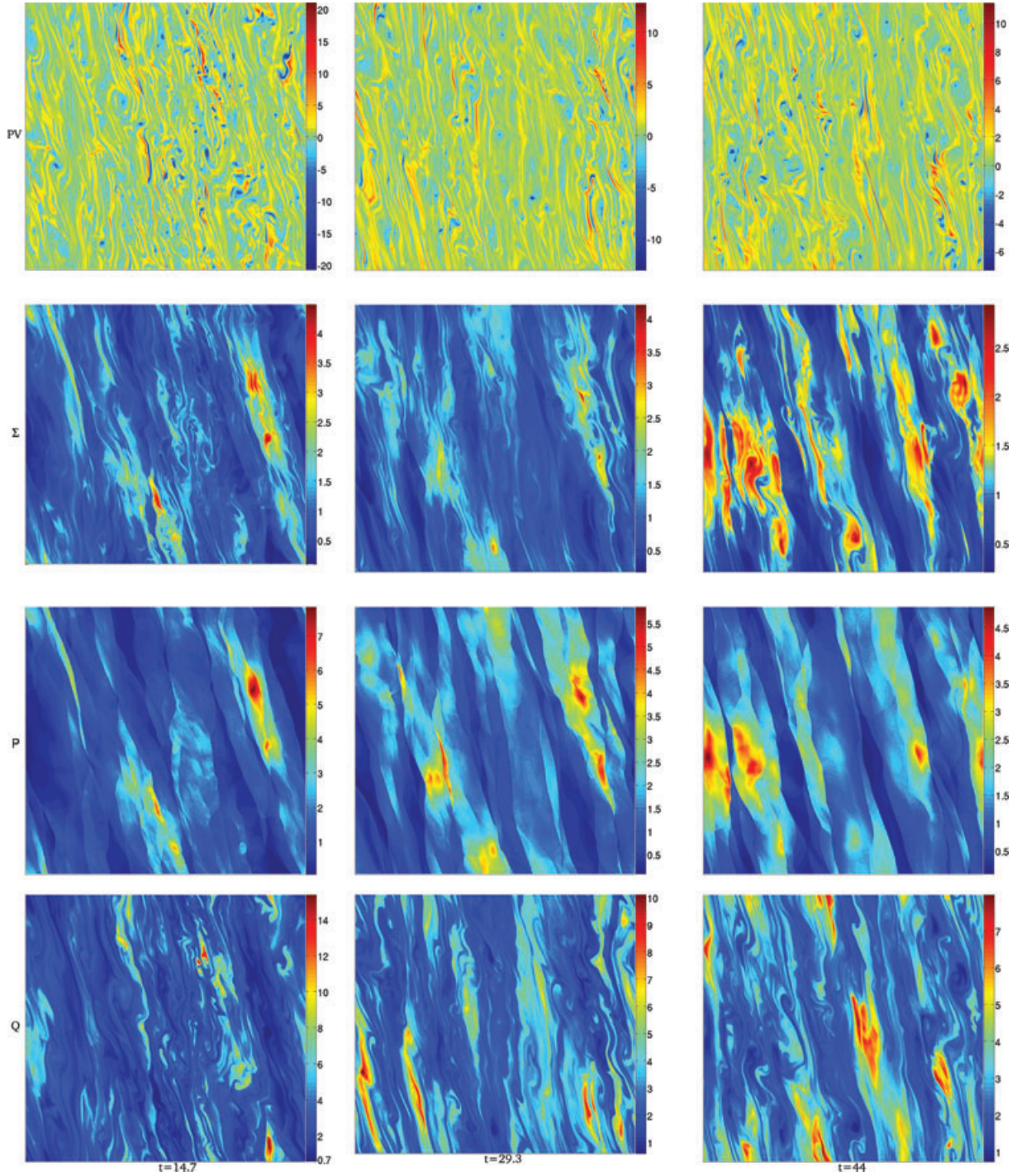


Figure 4. Evolution of PV, surface density, pressure/internal energy and Q parameter (from upper to lower rows, respectively) for the fiducial model in the gravitoturbulent state. Coordinate axes are same as in Fig. 1. Snapshots are at times $t = 14.7, 29.3, 44$. The PV field consists of vortices with different sizes and strengths (blue and light blue regions). Vortices with sizes smaller than the local Jeans scale have higher (by absolute value) negative PV centres (blue dots). They also emit density waves during evolution that turn into shocks. In the surface density field, these vortices correspond to underdense central regions surrounded by overdense regions marking density wave emission places that are characterized by smaller (by absolute value) than the central values of PV. In the Q field, the underdense and overdense regions give rise to high and low Q values, respectively, but the influence of self-gravity on such small-scale vortices is weak. The other type of vortices is somewhat larger having scales comparable to the local Jeans scale. They are more diffuse with no clear shape (light blue regions in PV field) and characterized by smaller (by absolute value) negative PV and stronger overdense regions (yellow and red in the surface density field) with even smaller Q than those in the previous case. For this reason, such vortices are in the process of being sheared and destroyed. In the pressure field, shocks and only the overpressure regions corresponding to stronger overdensities are notable (yellow and red). Exact values of these four quantities can be inferred from colour bars (see electronic edition of the journal for colour figures).

are also characterized by small Q values. In the pressure/internal energy field, we see shocks and only overpressure regions. The stronger overdensities (yellow and red in Fig. 4) associated with the final stage of vortex life (see below) clearly correlate with these overpressure regions. However, it is still hard to find as good a correspondence/similar features between PV and pressure/internal energy fields as it is for the surface density field. Nevertheless, in self-gravitating discs one can identify distinct features in the surface density and pressure/internal energy fields connected with vortices. By contrast, in analogous non-self-gravitating isothermal simulations, the situation is different. As mentioned above, similar density structures, i.e. with overdense and underdense regions, were also observed in numerical simulations of a single vortex before its settlement into an equilibrium configuration, where the anticyclonic vortex gives rise only to a single overdense region (Bodo et al. 2007). However, other simulations of vortex formation from an initial random distribution of PV (Johnson & Gammie 2005; Shen et al. 2006), which are not limited to only a single vortex, did not find overdense regions easily identifiable with individual vortices in the surface density field; there were only variations in the surface density due to the shocks shed by these vortices (see also Fig. 5). In our case instead, swing amplification due to self-gravity makes overdense and underdense regions clearly notable on the background of shocks.

Since $Q \leq 1$ at the location of the stronger overdense regions, self-gravity becomes dominant in the dynamics of vortices and appears to strongly shear and deform the latter over about $1-3\Omega^{-1}$ and most importantly to inhibit their further growth in size. In other words, self-gravity opposes an inverse cascade of energy to smaller wavenumbers and scatters it to higher wavenumbers. This fact is also reflected in the autocorrelation function of PV shown below (Fig. 6). The vortices can only grow to a size comparable to the local Jeans scale $\lambda_J \sim Qc_s$ (in non-dimensional variables). When the vortex size approaches the local Jeans scale, it has no clear centre with high (by absolute value) negative PV region surrounded by smaller (by absolute value) PV region and, therefore, corresponds only to the stronger overdense region (yellow and red regions in the surface density and pressure fields in Fig. 4) with no underdense centre. At this time, the shape of the vortex is more irregular, sheared and diffuse characterized by about 10 times smaller (by absolute value) PV than that of growing vortices. From the pressure/internal energy field, it is clear that in these stronger overdense regions the internal energy is higher as well and it is expected that corresponding Q will eventually rise and switch off self-gravity/gravitational instability at that location. Then the overdense region will quickly disperse, or get sheared away. After that sheared PV regions with higher Q , in turn, can start another cycle of vortex formation by undergoing the same non-linear Kelvin–Helmholtz instability and again wrap up into vortices. Thus, in self-gravitating discs, vortices have recurring nature – each vortex forms, grows to a size of the order of the local Jeans scale and after that gets sheared and destroyed by the combined effects of self-gravity and Keplerian shear. Each such a cycle typically lasts for about two orbital periods or less (one orbital period $=2\pi/\Omega$). Then sheared PV regions turn into vortices and after that the whole process starts again. The cooling ensures that the minimum Q_{\min} is kept low (0.6–0.7) and nearly constant with time, so that self-gravity continues to play a role.

Above we have described the behaviour of some individual vortices only. From Fig. 4, we see that the PV field contains vortices with different sizes that never get organized into distinct coherent vortices as they do in the non-self-gravitating case (Fig. 5). Vortices evolve differently – some of them are at the end of evolution having

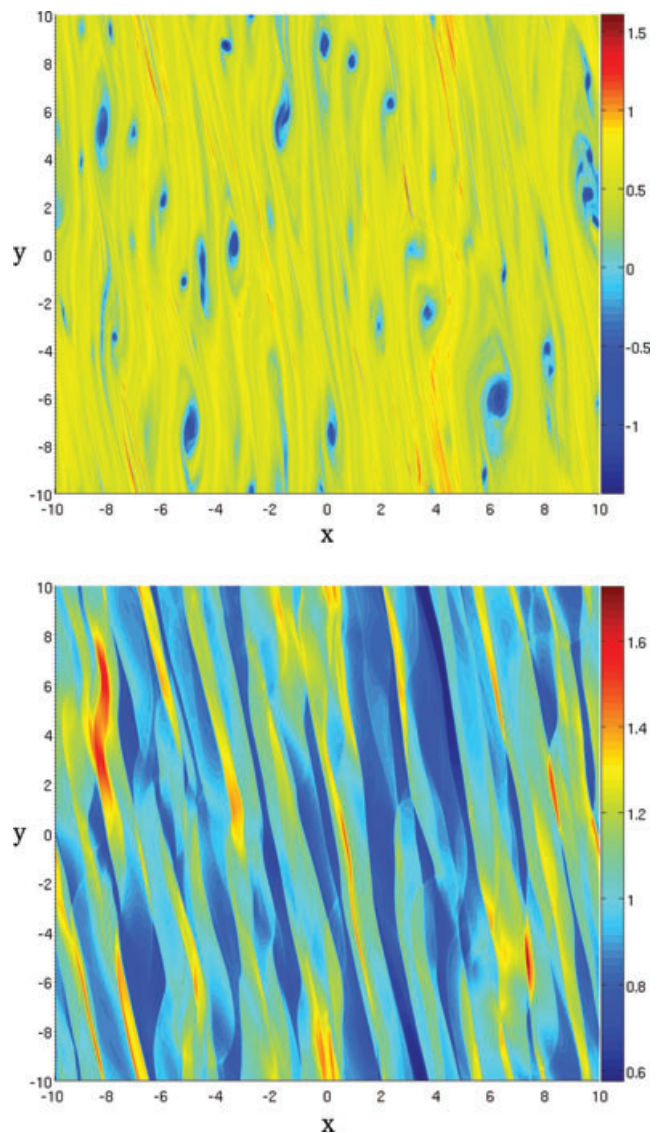


Figure 5. Typical PV field (upper plot) at $t = 44$ for the isothermal fiducial model with self-gravity switched off. The sound speed is equal to the average sound speed in the gravitoturbulent state (see Fig. 3). Also shown is the corresponding surface density field (lower plot). It is hard to see traces of individual vortices in the surface density field; only shocks shed by these vortices are visible. Vortices are organized into well-shaped larger scale structures as opposed to what is observed in the self-gravitating case in Fig. 4.

already grown to the Jeans scale sizes and characterized by clearly identifiable overdense regions and low Q , but others have yet to go through this phase and, therefore, may still have underdense central regions surrounded by higher density regions and correspond to higher Q . Thus, regions of high and low Q coexist throughout the disc at all times. A similar gravitoturbulent state was observed in the global disc simulations by Wada et al. (2002) in the context of interstellar medium turbulence. However, these authors did not measure PV corresponding to high- and low- Q regions. In general, the overall dynamical picture, as mentioned, is very irregular and it is hard to keep track of individual vortices for several orbital periods, because they are short-lived structures. Fig. 5 shows the stark contrast between non-self-gravitating and self-gravitating cases. In this figure, we present a snapshot of the same fiducial model, but without

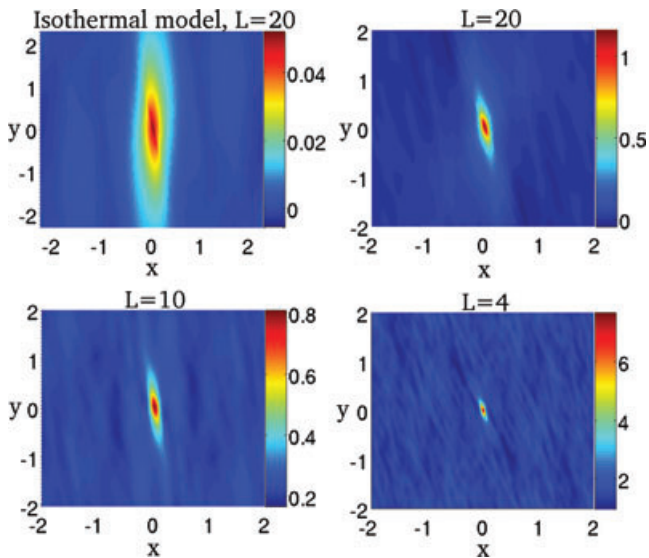


Figure 6. Autocorrelation functions of PV for four models: isothermal non-self-gravitating with $L = 20$ (Fig. 5) and three self-gravitating with $L = 20, 10, 4$ in the gravitoturbulent state. For the two fiducial models with the same $L = 20$, the correlation length is largest for the isothermal non-self-gravitating model and greatly decreases in the presence of self-gravity. It also decreases with decreasing L (see electronic version of the journal for colour figures).

self-gravity and with constant sound speed (isothermal equation of state) equal to the average sound speed of the fiducial model in the gravitoturbulent state (see Fig. 3). In this case, the dynamical picture is identical to that described by other authors (e.g. Umurhan & Regev 2004; Johnson & Gammie 2005; Shen et al. 2006). Now it is easier to trace each vortex and see how they merge into larger vortices. In the self-gravitating case, irregular and chaotic phases of vortex evolution are quasi-steady, or equivalently self-sustained during the entire course of evolution, whereas in the non-self-gravitating case, though vortices are well organized and regular, they gradually decay.

We also carried out simulations for two other models with sizes $L = 4$ and 10 and with the same type of initial conditions. The dynamical picture of vortex evolution described in detail for the fiducial model remains qualitatively the same. There are differences only in saturation times, and (average) values of various quantities in the gravitoturbulent state. In Fig. 6, we compare the autocorrelation functions of PV for these models with that of the non-self-gravitating isothermal model plotted in Fig. 5. The extent of the autocorrelation function, or the correlation length, remains on average unchanged with time in the gravitoturbulent state and does not depend on the spectrum of initial conditions. For the given model size $L = 20$, the correlation length is smaller than that in the non-self-gravitating case implying that vortices are less coherent in the gravitoturbulent state (we remind the reader that the sound speed of the isothermal model, determining the correlation length for this model, is equal to the average sound speed of the fiducial self-gravitating model). This again can be explained by the tendency of self-gravity to oppose inverse cascade of energy to larger scales by scattering it to smaller scales and thereby broadening the spectrum of the PV autocorrelation function. An alternative explanation is that in the self-gravitating case the contribution of Jeans scale size PV regions in the correlation function is smaller than that of smaller size PV regions. The correlation length appears to decrease

with decreasing model size, whereas in the isothermal case, it does not depend on the size of the model and is determined by the disc scale height (Johnson & Gammie 2005). In any case, correlation length is always smaller than the model size justifying the local treatment of vortices.

4 SUMMARY AND DISCUSSIONS

We have studied the specific properties of PV evolution in self-gravitating discs in the shearing sheet approximation. The evolution has been traced via numerical integration of the basic hydrodynamic equations supplemented with Poisson's equation taking care of self-gravity. Since we are interested particularly in the properties of vortex evolution in quasi-steady gravitoturbulence, we have chosen a simple cooling law with a constant cooling time large enough so that the disc settles down into this state. Our analysis has shown that in the self-gravitating case, vortices appear as transient structures undergoing recurring phases of formation, growth to sizes comparable to a local Jeans scale, and eventual shearing and destruction due to the combined action of self-gravity (gravitational instability) and background Keplerian shear. Each such a phase lasts for a few orbital periods. As a result, the overall dynamical picture is irregular, consisting of many transient vortices at different evolutionary stages and, therefore, with various sizes up to the local Jeans scale. By contrast, in the non-self-gravitating case, long-lived vortices form and grow in size via merging into larger ones until eventually their size reaches the disc scale height. The motion within vortices, or more precisely in the vicinity of negative PV regions, is a complex mixture of compressive (wave) and vortical motions which are difficult to separate from each other. Compressive motions turn into shocks afterwards, or equivalently, vortices appear to generate shocks. Therefore, the dynamics of compressive motions (density waves) and vortices are coupled implying that, in general, one should consider both vortex and spiral density wave modes to get a proper understanding of self-gravitating disc dynamics.

It is well known that overpressure/overdensity regions, if present in a disc, can act as traps for dust particles (e.g. Haghighipour & Boss 2003; Rice et al. 2004; Fromang & Nelson 2005; Rice et al. 2006; Lyra et al. 2009). As has been demonstrated in our simulations, in self-gravitating discs anticyclonic vortices, or generally negative PV regions, are able to produce quite notable overpressures/overdensities, though not long-lived. They have a transient character and vary on the dynamical time-scale. Hence, given such an irregular and rapidly changing nature of vortex evolution in self-gravitating discs, it seems difficult for corresponding overdensities/overpressures to effectively trap dust particles in their centres. Further study of a coupled system – dust particles embedded in a self-gravitating gaseous disc – is, however, required to strengthen this conclusion.

Here, we have considered the simplified case of a razor-thin (2D) disc in order to gain first insight into the effects of self-gravity on vortex dynamics. Obviously, for a fuller understanding 3D treatment is necessary. The situation can be different in the 3D self-gravitating case, which is evidently stratified in the vertical direction. Barranco & Marcus (2005) demonstrated that in the 3D non-self-gravitating stratified shearing box, off-mid-plane vortices appear and survive for many orbital periods. A similar 3D study by Shen et al. (2006), but not including stratification, showed that vortices are unstable and get quickly destroyed due to an elliptical instability. So, it can be said that the presence of stratification helps the survival of vortices. On the other hand, as we have seen here, self-gravity does not favour long-lived vortices. But in the 3D case, the effect of self-gravity is

somewhat reduced compared with that in the 2D case considered here. Thus, in a 3D generalization of the present problem there are two competing factors – stratification and self-gravity – and it remains to be seen in numerical experiments which of these two prevails. Another question of interest in the 3D case (either self-gravitating or not) is, as also pointed out by Johnson & Gammie (2005), if long-lived off-mid-plane vortices can be generated from a random PV distribution, as happens in the 2D case, rather than from specially chosen vortex solutions as in simulations of Barranco & Marcus (2005).

ACKNOWLEDGMENTS

GRM would like to acknowledge the financial support from the Scottish Universities Physics Alliance (SUPA). He also thanks G. D. Chagelishvili and A. G. Tevzadze for helpful discussions and reading the manuscript. The original version of the ZEUS code suited for the shearing sheet as well as useful comments and suggestions regarding numerical simulations of vortices in discs were kindly provided by C. F. Gammie.

REFERENCES

- Adams F. C., Lin D. N. C., 1993, in Levy E. H., Lunine J. I., eds, *Protostars and Planets III*. Univ. Arizona Press, Tucson, p. 721
- Adams F. C., Watkins R., 1995, *ApJ*, 451, 314
- Barge P., Sommeria J., 1995, *A&A*, 295, L1
- Barranco J. A., Marcus P. S., 2005, *ApJ*, 623, 1157
- Bertin G., Lodato G., 2001, *A&A*, 370, 342
- Bodo G., Chagelishvili G., Murante G., Tevzadze A., Rossi P., Ferrari A., 2005, *A&A*, 437, 9
- Bodo G., Tevzadze A., Chagelishvili G., Mignone A., Rossi P., Ferrari A., 2007, *A&A*, 475, 51
- Boley A. C., Meija A. C., Durisen R. H., Cai K., Pickett M. K., D’Alessio P., 2006, *ApJ*, 651, 517
- Bracco A., Chavanis P. H., Provenzale A., Spiegel E., 1999, *Phys. Fluids*, 11, 2280
- Chavanis P. H., 2000, *A&A*, 356, 1089
- Davis S. S., 2002, *ApJ*, 576, 450
- Davis S. S., Sheehan D. P., Cuzzi J. N., 2000, *ApJ*, 545, 494
- Durisen R. H., Boss A. P., Mayer L., Nelson A. F., Quinn T., Rice W. K. M., 2007, in Reipurth B., Jewitt D., Keil K., eds, *Protostars and Planets V*. University of Arizona Press, Tucson, p. 607
- Fromang S., Nelson R., 2005, *MNRAS*, 364, L81
- de la Fuente Marcos C., Barge P., 2001, *MNRAS*, 323, 601
- Gammie C., 2001, *ApJ*, 553, 174
- Godon P., Livio M., 1999a, *ApJ*, 521, 319
- Godon P., Livio M., 1999b, *ApJ*, 523, 350
- Godon P., Livio M., 2000, *ApJ*, 537, 396
- Goldreich P., Lynden-Bell D., 1965, *MNRAS*, 130, 125
- Goldreich P., Tremaine S., 1978, *ApJ*, 222, 850
- Haghighipour N., Boss A. P., 2003, *ApJ*, 583, 996
- Hawley J. F., Gammie C. F., Balbus S. A., 1995, *ApJ*, 440, 742
- Inaba S., Barge P., 2006, *ApJ*, 649, 415
- Johansen A., Andersen A. C., Brandenburg A., 2004, *A&A*, 417, 361
- Johansen A., Oishi J. S., Mac Low M. M., Klahr H., Henning T., Youdin A., 2007, *Nat*, 448, 1022
- Johnson B. M., Gammie C. F., 2003, *ApJ*, 597, 131
- Johnson B. M., Gammie C. F., 2005, *ApJ*, 635, 149
- Kim W., Ostriker E., 2001, *ApJ*, 559, 70
- Klahr H. H., 2004, *ApJ*, 606, 1070
- Klahr H. H., Bodenheimer P., 2003, *ApJ*, 582, 869
- Klahr H. H., Bodenheimer P., 2006, *ApJ*, 639, 432
- Laughlin G., Bodenheimer P., 1994, *ApJ*, 436, 335
- Laughlin G., Korchagin V., Adams F. C., 1997, *ApJ*, 477, 410
- Li H., Colgate S. A., Wendroff B., Liska R., 2001, *ApJ*, 551, 874
- Lithwick Y., 2007, *ApJ*, 670, 789
- Lodato G., 2007, *La Rivista del Nuovo Cimento*, 30, 293
- Lodato G., Rice W. K. M., 2004, *MNRAS*, 351, 630
- Lodato G., Rice W. K. M., 2005, *MNRAS*, 358, 1489
- Lovelace R. V. E., Li H., Colgate S. A., Nelson A. F., 1999, *ApJ*, 513, 805
- Lyra W., Johansen A., Klahr H., Piskunov N., 2009, *A&A*, 493, 1125
- Mamatsashvili G. R., Chagelishvili G. D., 2007, *MNRAS*, 381, 809
- Masset F., 2000, *A&AS*, 141, 165
- Meija A. C., Durisen R. H., Pickett M. K., Cai K., 2005, *ApJ*, 619, 1098
- Nelson A. F., Benz W., Ruzmaikina T. V., 2000, *ApJ*, 529, 357
- Petersen M. R., Julien K., Stewart G. R., 2007, *ApJ*, 658, 1236
- Rice W. K. M., Armitage P. J., Bate M. R., Bonnell I. A., 2003, *MNRAS*, 339, 1025
- Rice W. K. M., Lodato G., Pringle J. E., Armitage P. J., Bonnell I. A., 2004, *MNRAS*, 355, 543
- Rice W. K. M., Lodato G., Pringle J. E., Armitage P. J., Bonnell I. A., 2006, *MNRAS*, 372, L9
- Shen Y., Stone J. M., Gardiner T. A., 2006, *ApJ*, 653, 513
- Stamatellos D., Whitworth A. P., 2008, *A&A*, 480, 879
- Stone J. M., Norman M. L., 1992, *ApJS*, 80, 753
- Toomre A., 1964, *ApJ*, 139, 1217
- Toomre A., 1981, in Fall S. M., Lynden-Bell D., eds, *The Structure and Evolution of Normal Galaxies*. Cambridge Univ. Press, Cambridge, p. 111
- Umurhan O. M., Regev O., 2004, *A&A*, 427, 855
- Wada K., Meurer G., Norman C., 2002, *ApJ*, 577, 197

This paper has been typeset from a $\text{\TeX}/\text{\LaTeX}$ file prepared by the author.